Ferromagnetic Interactions between Imino Nitroxides through Diamagnetic Metal Ions: Crystal Structures, Magnetism, and Electronic Properties of [M^I(imino nitroxide)$_2$](PF_6) (M = Cu^I and Ag^I)

Hiroki Oshio,*,† Takashi Watanabe,† Akihiro Ohto,† Tasuku Ito,† Tadaaki Ikoma,‡ and Shozo Tero-Kubota‡

Department of Chemistry, Graduate School of Science, Tohoku University, Aoba-ku, Sendai 980-77, Japan, and Institute for Chemical Reaction Science, Tohoku University, Aoba-ku, Sendai 980-77, Japan

Received August 1, 1996[⊗]

An orthogonal arrangement of imino nitroxide ligands in Cu^I and Ag^I complexes results in propagation of an intramolecular ferromagnetic interaction between the coordinated imino nitroxides through these diamagnetic ions. Reaction of [$Cu^I(CH_3CN)_4$](PF_6) and $Ag^I(PF_6)$ with imino nitroxides in ethanol solution gave [Cu^I(immepy)$_2$](PF_6) (**1**) and [Ag^I(impy)$_2$](PF_6) (**2**), respectively (immepy = 2-(2-(6-methylpyridyl))-4,4,5,5-tetramethyl-4,5-dihydro-1*H*-imidazolyl-1-oxy and impy = 2-(2-pyridyl)-4,4,5,5-tetramethyl-4,5-dihydro-1*H*-imidazolyl-1-oxy). Complex **1** crystallizes in the orthorhombic space group *Pba*2, which has a unit cell with $a = 11.251(2)$ Å, $b = 14.745(3)$ Å, $c = 9.747(2)$ Å, $V = 1617.0(5)$ Å^3, and $Z = 2$. Refinement with 991 reflections observed [$|I_o| > 3\sigma(I_o)$] gave $R = 0.044$ ($R_w = 0.053$). In **1**, imino nitroxides coordinate to the Cu^I ions in a tetrahedral fashion, the dihedral angle between coordinating imino nitroxides being 88.7°. Magnetic susceptibility measurement for **1** shows typical triplet−singlet behavior with strong ferromagnetic interactions ($J = 55.1(6)$ cm^{-1} with $g = 2.0$; $H = -JS_1 \cdot S_2$). The UV−visible absorption spectrum of **1** shows strong bands at 464 and 766 nm assignable to charge-transfer bands from the Cu ion to the ligand NLUMO and SOMO, respectively. The π-back-donation to the SOMO induces the spin on the Cu ion and results in the strong ferromagnetic interaction. Complex **2** crystallizes in the orthorhombic space group $P2_1cn$ which has a unit cell with $a = 10.535(6)$ Å, $b = 31.295(3)$ Å, $c = 8.921(4)$ Å, $V = 2941(1)$ Å^3, and $Z = 4$. Refinement with 1882 reflections [$|I_o| > 3\sigma(I_o)$] gave $R = 0.058$ ($R_w = 0.074$). In **2**, the four coordination sites of the Ag^I ion were completed with two imino nitroxides and the dihedral angle between the imino nitroxides is 79.2°. The EPR spectrum of a frozen ethanol solution of **2** shows a typical triplet signal with zero field splitting ($|D| = 0.043$ cm^{-1} and $|E| = 0.014$ cm^{-1}). Curie plots for the $\Delta m = 2$ signal below 80 K gave a positive Weiss constant ($\theta = 4$ K), suggesting an intramolecular ferromagnetic interaction in **2**.

Introduction

Magnetic interactions within or between molecules are typically antiferromagnetic, at best in accord with molecular orbital considerations. However, ferromagnetic interactions can arise in several ways.[1] (i) Orthogonal arrangement of the magnetic orbitals can lead to stabilization of the high-spin state, such situation being observed for metal complexes and metal−radical complexes.[2] (ii) Spin polarization, a strategy originally suggested by McConnell,[3] and later documented for intermolecular stacks having complementary spin alignment, can lead to ferromagnetic interaction.[4] (iii) Topological symmetry of the π-electron network can be applied to design high spin organic molecules such as polycarbenes.[5] (iv) Configurational mixing of a ground high spin with charge-transfer configurations stabilizes the high-spin ground state.[6] It should be noted that the easiest way to achieve ferromagnetic interactions is the approach based on the orthogonality of magnetic orbitals. In addition to the orthogonality, the existence of direct or indirect charge-transfer interactions between the paramagnetic centers can generate or enhance ferromagnetic interactions, such effects being most conveniently treated with a valence bond-like approach.

Typically, magnetic interactions between paramagnetic centers through diamagnetic metal ions are negligibly small or weakly antiferromagnetic. Trinuclear systems such as dimethylglyoximato-bridged $Cu^{II}-Ni^{II}(LS)-Cu^{II}$ [7] and $Fe^{III}-Fe^{II}(LS)-Fe^{III}$ [8] (LS = low spin) complexes show weak antiferromagnetic interactions ($J = -2.6$ and -4.4 cm^{-1}, respectively) between

† Department of Chemistry.
‡ Institute for Chemical Reaction Science.
⊗ Abstract published in *Advance ACS Abstracts,* June 1, 1997.

(1) (a) Kollmar, C.; Kahn, O. *Acc. Chem. Res.* **1993**, *26*, 259. (b) Miller, J. S.; Epstein, A. J. *Angew. Chem., Int. Ed. Engl.* **1994**, *33*, 385.
(2) (a) Kahn, O; Galy, J.; Journaux, Y.; Jaud, J.; Morgenstern-Badarau, I. *J. Am. Chem. Soc.* **1982**, *104*, 2165. (b) Pei, Y.; Journaux, Y.; Kahn, O. *Inorg. Chem.* **1989**, *28*, 100. (c) Caneschi, A.; Gatteschi, D.; Laugier, J.; Rey, P. *J. Am. Chem. Soc.* **1987**, *109*, 2191. (d) Tamaki, H.; Zhong, Z. J.; Matsumoto, N.; Kida, S.; Koikawa, M.; Achiwa, N.; Hashimoto, Y.; Okawa, S. *J. Am. Chem. Soc.* **1992**, *114*, 6974. (d) Oshio, H.; Nagashima, U. *Inorg. Chem.* **1992**, *31*, 3295.
(3) McConnel, H. M. *J. Chem Phys.* **1963**, *39*, 1910.
(4) (a) Miller, J. S.; Epstein, A. J.; Reiff, W. M. *Acc. Chem. Res.* **1988**, *21*, 114. References therein. (b) Kollmar, C.; Vouty, M.; Kahn. O. *J. Am. Chem. Soc.* **1991**, *113*, 7994. (b) Izuoka, A.; Murata, S.; Sugawara, T.; Iwamura, H. *J. Am. Chem. Soc.* **1987**, *109*, 2631.
(5) (a) Sugawara, T.; Bandow, S.; Kimura, K. Iwwamura, H.; Itoh, K. *J. Am. Chem. Soc.* **1986**, *108*, 368. (b) Teki, Y.; Takui, T.; Itoh, K. Iwamura, H.; Kobayashi, K. *J. Am. Chem. Soc.* **1986**, *108*, 2147. (c) Fujita, I.; Teki, Y.; Takui, T.; Kinoshita, T. Itoh, K. *J. Am. Chem. Soc.* **1990**, *112*, 4074.
(6) (a) Miller, J. S.; Calabrese, J. C.; Rommelmann, H. Chittipeddi, R.; Zhang, J. H.; Reiff, W. M.; Epstein, A. J. *J. Am. Chem. Soc.* **1987**, *109*, 769. (b) Turek, P.; Nozawa, K.; Shimoi, D.; Awaga, K.; Inabe, T.; Maruyama, Y.; Kinoshita, M. *Chem. Phys. Lett.* **1991**, *180*, 327.
(7) Chaudhuri, P.; Winter, M.; Della Védova, B. B. C.; Bill, E.; Trautwein, A.; Gehring S.; Fleischhauer, P.; Nuber, B.; Weis, J. *Inorg. Chem.* **1991**, *30*, 2148.

S0020-1669(96)00939-1 CCC: $14.00

the terminal metal ions. However, a moderately strong antiferromagnetic interaction ($J = -36$ cm^{-1}) has been observed for an analogous Cu^{II}−Pd^{II}−Cu^{II} complex.[7] In contrast to the paramagnetic metal complexes, diamagnetic metal complexes with semiquinones show a variety of magnetic interactions depending on metal ions and coordination geometries. A series of square planar metal complexes [M(SQ)$_2$] (M = Ni, Pd, and Pt) (SQ = *tert*-butyl-substituted semiquinone) shows fairly strong antiferromagnetic interactions due to indirect overlap of the magnetic orbitals through the metal dπ orbitals.[9] The strength of inter-radical exchange increases down the series of metal ions; i.e., the strongest coupling is for Pt and the weakest for Ni. On the other hand, pseudo-octahedral coordination geometry provides for orthogonal coordination of semiquinones. [M^{III}(3,6-DBSQ)$_3$][10] (M = Al and Ga; 3,6-DBSQ = 3,6-di-*tert*-butylsemiquinone) and [Ga^{III}(3,5-dtbsq)$_3$][11] (3,5-dtbsq = 3,5-di-*tert*-butyl-1,2-benzosemiquinone) showed weak ferromagnetic interactions ($J = 6.2$, 8.6, and 7.8 cm^{-1}, where $H = -2J\Sigma S_i \cdot S_j$), while [M^{IV}(Cat−N-SQ)$_2$] (M = Ti, Ge, and Sn) (Cat−N-SQ = tridentate Schiff base biquinone)[12] were characterized by a triplet ground state with the exchange coupling constants of $J = -56$, -27, and -23 cm^{-1} ($H = J\Sigma S_1 \cdot S_2$), respectively. It should be noted that the magnitude of magnetic interactions through diamagnetic ions depend strongly on the energy of the dπ orbitals.

Which diamagnetic metal complex provides the appropriate symmetry and orbital energy to propagate ferromagnetic interaction? Ab initio molecular orbital calculations of the divalent metal oxides have proven that, among the first-row transition metal ions, d-orbital energy of the Cu ion is the closest to the oxygen p-orbital.[13] Furthermore, an XPS study of [2,5-DM-DCNQI]$_2$Cu (2,5-DM-DCNQI = 2,5-dimethyl−*N*,*N*′-dicyanoquinonediimine),[14] which shows conducting properties, has revealed that the Cu ion is in the mixed-valence state and the mix valency plays an important role in the conductivity of the DCNQI column.[15] It is, therefore, expected that the Cu ion has an appropriate d-orbital energy to interact with the organic π-orbitals. In addition, Cu(I) ions are known to favor a tetrahedral coordination geometry,[16] which is suitable for the orthogonal arrangement of two bidentate ligands. Thus, it is anticipated that coordination of two bidentate radical ligands to the Cu(I) ion would lead to a ferromagnetic interaction between the radicals. This expectation is herein confirmed for the Cu(I) complex of a bidentate imino nitroxide (L), [CuL$_2$]$^+$. Specifically, in this work, we synthesized Cu(I) and silver(I) complexes of general formula [M(L)$_2$](PF$_6$), where L is the bidentate imino nitroxide immepy or imy, and their magnetic properties were discussed. In addition to the study of their magnetic susceptibility measurements, EPR and electronic spectra were used together with electrochemical measurements, which provide information about electronic structures of the complexes. A preliminary communication of the structure and magnetic property of the Cu(I) complex has been already published.[17]

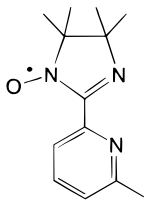

immepy

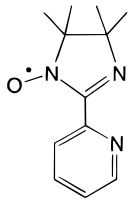

impy

Experimental Section

Syntheses. All chemicals (Wako Chemicals, Ltd.) were used as received without further purification. Imino nitroxides[18] and [Cu^{I}(CH$_3$CN)$_4$](PF$_6$)[19] were prepared by the literature methods.

[Cu^{I}(immepy)$_2$](PF$_6$) (1). All procedures were carried out under a nitrogen atmosphere. A solution of immepy (0.23 g, 1.0 mmol) in ethanol (10 mL) was added to a solution of [Cu^{I}(CH$_3$CN)$_4$](PF$_6$) (0.19 g, 0.5 mmol) in ethanol (15 mL). After the solution was left standing overnight, dark red tablets were filtered out by suction and one of them was subjected to the X-ray analysis. Anal. Calcd for C$_{26}$H$_{36}$CuF$_6$N$_6$O$_2$P: C, 46.39; H, 5.39; N, 12.49. Found: C, 46.20; H, 5.19; N, 12.47.

[Ag^{I}(impy)$_2$](PF$_6$) (2). Ag^{I}(PF$_6$) (0.25 g, 0.1 mmol) dissolved in methanol (30 mL) was added to a solution of impy (0.44 g, 0.2 mmol) in methanol (10 mL). The resulting red crystalline solid was collected by filteration. Recrystallization from hot ethanol gave red needlelike crystals, and one of them was subjected to X-ray analysis. Anal. Calcd for C$_{24}$H$_{32}$AgF$_6$N$_6$O$_2$P: C, 41.81; H, 4.68; N, 12.19. Found: C, 41.26; H, 4.67; N, 12.10.

Magnetic Measurement. Magnetic susceptibility data were collected in the temperature range 2.0−300 K and in an applied 10 K G field with the use of a Quantum Design Model MPMS SQUID magnetometer. Powdered samples were contained in the small half of a gelatin Capsule, and a phenolic guide (a clear soda straw) was used to house the sample holder and was fixed to the end of the magnetometer drive rod. Pascal's constants[20] were used to determine the constituent atom diamagnetism.

EPR Measurement. The X-band and Q-band EPR spectra of frozen ethanol solutions were recorded at various temperatures between 5.0 and 80 K with a Bruker spectrometer (ESP-300E), which was equipped with a helium continuous-flow cryostat, a Hall probe, and a frequency meter.

X-ray Crystallography. Single crystals of **1** and **2** were mounted on the tips of glass fibers with epoxy resin. Diffraction data were collected on a Rigaku 5R four-circle diffractometer equipped with liquid-N$_2$ cryostream cooler (Oxford Cryosystems). Graphite-monochromatized Cu Kα radiation (1.541 78 Å) for **1** and Mo Kα radiation ($\lambda = 0.710\ 69$ Å) for **2** were respectively used for the measurements. All data were corrected for Lorentz and polarization effects, and empirical absorption corrections (ψ-scans) were carried out in each case. No decay in intensity was observed during measurements. The lattice constants for **1** and **2** were optimized from a least-squares refinement of the settings for 25 carefully centered Bragg reflections in the range of $50° < 2\theta < 80°$ and $25° < 2\theta < 30°$, respectively. Crystallographic data are collected in Table 1. The structures were

(8) Chaudhuri, P.; Winter, M.; Fleischhauer, P.; Haase, W.; Flörke, U.; Haupt, H. J. *J. Chem. Soc., Chem. Commun.* **1990**, 1728.
(9) (a) Fox, G. A.; Pierpont, C. G. *Inorg. Chem.* **1992**, *31*, 3718. (b) Abakumov, G. A.; Cherkasov, V. K.; Bubnov, M. P.; Ellert, O. G.; Rakitin, U. V.; Zakharov, L. N.; Struchkov, Y. T.; Saf'yanov, U. N. *Isv. Akad. Nauk SSSR* **1992**, 2315.
(10) Lange, C. W.; Conklin, B. J.; Pierpont, C. G. *Inorg. Chem.* **1994**, *33*, 1276.
(11) (a) Adams, D. M.; Rheingold, A. L.; Dei, A.; Hendrickson, D. N. *Angew. Chem., Int. Ed. Engl.* **1993**, *32*, 391. (b) Ozarowski, A.; Mcgarvey, B. R.; El-Hadad, A.; Tian, Z.; Tuck, D. G.; Krovich, D. J.; DeFtis, G. C. *Inorg. Chem.* **1993**, *32*, 841.
(12) Bruni, S.; Caneschi, A.; Cariati, F.; Delfs, C.; Dei, A.; Gatteschi, D. *J. Am. Chem. Soc.* **1994**, *116*, 1388.
(13) Yamaguchi, K.; Nakano, M.; Namimoto, H.; Fueno, T. *Jpn. J. Appl. Phys.* **1988**, *27*, L1835.
(14) Aumuller, A.; Erk, P.; Klebe, G.; Hünig, S.; von Schütz, J. U.; Werner, H-P. *Angew. Chem., Int. Ed. Engl.* **1986**, *25*, 740.
(15) Kobayashi, A.; Kato, R.; Kobayashi, H.; Mori, T.; Inokuchi, H. *Solid State Commun.* **1987**, *64*, 45.
(16) Cotton, F. A.; Wilkinson, G. *Advanced Inorganic Chemistry, 5th ed.*; Wiley: New York, 1988.
(17) Oshio, H.; Watanabe, T.; Ohto, A.; Ito, T.; Nagashima, U. *Angew. Chem., Int. Ed. Engl.* **1994**, *33*, 670.
(18) Caneschi, A.; Gatteschi, D.; Rey, P. *Prog. Inorg. Chem.* 1**991**, *39*, 331.
(19) Kubas, G. J.; Monzyk, B.; Crumbliss, A. L.; *Inorg. Synth.* **1989**, *19*, 90.
(20) Hatfield, W. E. *Theory and Application of Molecular Paramagnetism*; Boudreaux, E. A., Mulay, L. N., Eds.; Wiley and Sons, Inc.: New York, 1976; pp 491−495.

Table 1. Crystal and Refinement Data for $[Cu(immepy)_2](PF_6)$ (**1**) and $[Ag(impy)_2](PF6)$ (**2**)

	(**1**)	(**2**)
formula	$C_{26}H_{36}CuF_6N_6O_2P$	$C_{24}H_{32}AgF_6N_6O_2P$
fw	673.12	689.39
temp (°C)	−50	22
cryst system	orthorhombic	orthorhombic
space group	*Pba*2	$P2_1cn$
a (Å)	11.251(2)	10.535(6)
b (Å)	14.745(3)	31.295(3)
c (Å)	9.747(2)	8.921(4)
U (Å^3)	1617.0(5)	2941(1)
Z	2	4
D_{calc} (g cm^{-3})	1.382	1.557
radiation (Å)	1.541 78	0.710 69
μ(Cu Kα), μ(Mo Kα) (cm^{-1})	4.82 (Cu)	7.93 (Mo)
tot. data collcd	1131	3612
indepdt data, $\lvert I_o\rvert > 3\sigma(I_o)$	991	1882
tot. variables	191	396
transm. coeff.	0.765−0.971	0.943−0.991
R^a	0.044	0.058
$R_w{}^b$	0.053	0.074
weighting function	$(\sigma_c{}^2 + (0.020\lvert F\rvert)^2)^{-1}$	$(\sigma_c{}^2 + (0.020\lvert F\rvert)^2)^{-1}$

^{a} $R = \sum(\lvert F_o\rvert - \lvert F_c\rvert)/\sum\lvert F_o\rvert$. ^{b} $R_w = [\sum w(\lvert F_o\rvert - \lvert F_c\rvert)^2/\sum w\lvert F_o\rvert^2]^{1/2}$.

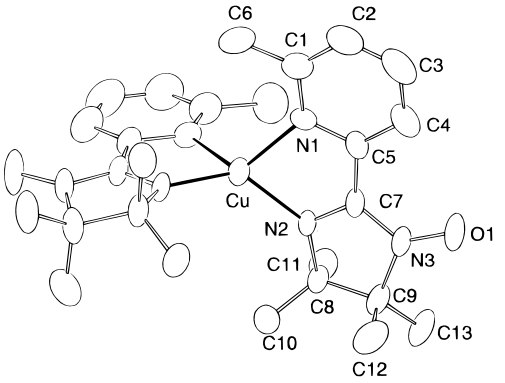

Figure 1. ORTEP drawing of $[Cu^I(immepy)_2]^+$.

solved by direct methods with SHELX-S86[21] and Fourier techniques and refined by the full-matrix least-squares method using XTAL 3.2.[22] All non-hydrogen atoms were readily located and refined with anisotropic thermal parameters. The structures of both complexes are noncentrosymmetric. The noncentrosymmetric structure and its inversion were refined successfully using the complete data set of all observed reflections and 191 (for **1**) and 396 (for **2**) variable parameters. The final R/R_w values of the structures presented here for **1** and **2** were calculated to be 0.044/0.053 and 0.058/0.074, those for the inversions being 0.046/0.057 and 0.060/0.076, respectively. Atomic positional parameters, along with full lists of bond lengths and angles, are available as Supporting Information.

Electrochemical Measurement and UV−Vis Spectra. Cyclic voltammetry (cv) measurements were accomplished with a three-electrode potentiostat (Hokuto Denko HA501G potentiostat/galvanostat and HB-105 function generator). Internal resistance drop was compensated with a Hokuto HI-203 IR compensation instrument for cv. The electrochemical measurements were performed in a microcell at 25 °C with the use of a conventional three-electrode configuration consisting of a highly polished glassy carbon working electrode (area 0.28 cm^3; BAS Ltd.), a platinum-wire auxiliary electrode, and an Ag/AgCl reference electrode containing 3 mol dm^{-3} NaCl solution (BAS Ltd.). Spectral grade acetonitrile (Dojin Lab.) was used without further purification. The supporting electrolyte $[N(Bu)_4](PF_6)$ (Fluka Chemie AG Industries) was recrystallized two times from ethanol and water and dried under vacuum in an oven at 80 °C for 12 h. The cell compartment was bubbled with solvent-saturated nitrogen to deaerate the solution. Ferrocene was used as an internal standard. Potentials for the compound are reported vs corrected Ag/AgCl. The half-wave potential of the ferrocene−ferrocenium couple under the conditions employed was 0.45 V ($\Delta E_p = 60$ mV) vs Ag/AgCl. Electronic spectra were recorded on an Hitachi U-3400 spectrophotometer.

Molecular Orbital Calculations. A molecular orbital calculations for the imino nitroxide ligands were carried out using the PM3 Hamiltonian and a RHF method in MOPAC, Ver. 6.00 (QCPE No. 445).[23]

Table 2. Selected Bond Lengths (Å) and Angles (deg) of $[Cu(immepy)_2]PF_6$ (**1**)

Cu−N1	2.081(6)	Cu−N2	1.953(5)
O1−N3	1.273(7)	N2−C7	1.271(7)
N3−C7	1.374(8)		
N1−Cu−N2	81.1(2)	N1−Cu−N1^a	116.8(2)
N1−Cu−N2^a	126.0(2)	N2−Cu−N2^a	131.2(2)
Cu−N1−C1	128.4(6)	Cu−N1−C5	111.9(4)
C1−N1−C5	119.7(7)	Cu−N2−C7	114.2(4)
Cu−N2−C8	135.3(4)	N2−C7−N3	112.5(6)
O1−N3−C7	126.1(7)		

^{a} Key to symmetry operation: $1 - x$, $1 - y$, z.

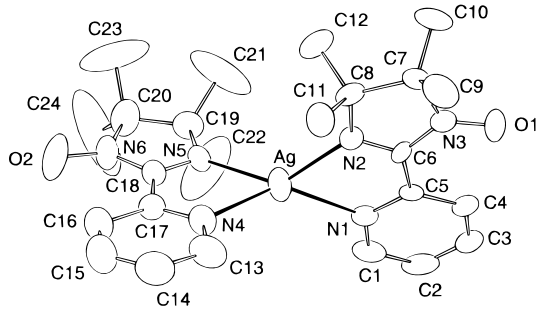

Figure 2. ORTEP drawing of $[Ag^I(impy)_2]^+$.

Results

Description of the Structure. $[Cu^I(immepy)_2](PF_6)$ (1). The structure of $[Cu^I(immepy)_2]^+$ is shown in Figure 1, and selected bond lengths and angles are given in Table 2. Complex **1** crystallizes in the orthorhombic space group *Pba*2, and both the cation and the anion are positioned on the 2-fold axis. A Cu ion, which is located on the C_2 axis, is coordinated by the crystallographically equivalent immepy ligands acting as bidentate ligands. The coordination geometry about Cu ion is pseudotetrahedral with the four coordination sites of the Cu ion being occupied by four nitrogen atoms. The Cu−N(imino nitroxide) bond is slightly shorter (1.953(5) Å) than the Cu−N(pyridine) bond (2.081(6) Å). The Cu ion lies at a mean distance of 0.08(1) and 0.14(1) Å above radical plane (N2−C7−N3-O1) and pyridine ring, receptively. Chelation of immepy leads to coplanarity of the imino nitroxide fragnments (N2−C7−N3−O1) and the pyridine plane of which the dihedral angle is 2.9(6)°. It should be noted that the two radical planes (magnetic orbitals) coordinated to the Cu ion in **1** are perpendicular to each other with the measured dihedral angle being 88.7°.

$[Ag^I(impy)_2](PF_6)$ (2). The ORTEP drawing of $[Ag^I(impy)_2]^+$ is shown in Figure 2, and selected bond lengths and angles are given in Table 3. Complex **2** crystallizes in the orthorhombic space group $P2_1cn$. Four of the fluorine atoms of the PF_6^- ion are positionally or rotationally disordered around the F−P−F axis. Four nitrogen atoms from two impy ligands coordinate to the silver ion in a distorted tetrahedral fashion.

(21) Sheldrick, G. M. *SHELXS-86*; University of Göttingen: Göttingen, Germany, 1986.
(22) Hall, S. R.; Sterwart, J. M. *XTAL3.2*; Universities of Western Australia and Maryland: Nedlands, Australia, and College Park, MD, 1992.
(23) Stewart, J. J. *QCPE Bull.* **1990**, *10* (4), 86.

Table 3. Selected Bond Lengths (Å) and Angles (deg) of [Ag(impy)$_2$]PF6 (**2**)

Ag−N1	2.351(8)	Ag−N2	2.245(9)
Ag−N4	2.400(9)	Ag−N5	2.211(9)
N2−C6	1.28(1)	N3−C6	1.40(1)
N5−C18	1.26(1)	N6−C18	1.38(2)
O1−N3	1.23(2)	O2−N6	1.29(2)
N1−Ag−N2	72.3(3)	N1−Ag−N4	139.3(4)
N1−Ag−N5	129.6(3)	N2−Ag−N4	120.3(3)
N2−Ag−N5	134.3(3)	N4−Ag−N5	72.0(3)
Ag−N1−C1	125.8(8)	Ag−N1−C5	114.6(6)
Ag−N2−C6	115.9(7)	Ag−N2−C8	130.2(7)
Ag−N4−C13	126(1)	Ag−N4−C17	113.8(8)
Ag−N5−C18	117.4(8)	Ag−N5−C19	131.5(7)
O1−N3−C6	126(1)	O2−N6−C18	126(1)
N2−C6−N3	111.7(9)	N5−C18−N6	112(1)

The average bond lengths between the silver ion and the coordinated nitrogen atoms are 2.375 and 2.228 Å for Ag−N(pyridine) and Ag−N(imino nitroxide), respectively, which are much longer than those of the Cu complex. The silver ion is slightly displaced (0.073 and 0.096 Å) from the mean planes of the radicals (defined as N2−C6−N3−O1 and N5−C18−N6−O2). The dihedral angle between the two radical planes is 79.2°.

Magnetic Properties. [Cu^{I}(immepy)$_2$](PF$_6$) (1). The magnetic susceptibility data for **1** are shown in Figure 3, in the form of the $\chi_m T$ versus T plot, where χ_m is the molar magnetic susceptibility. In **1**, there are two imino nitroxides coordinated to a diamagnetic Cu ion; hence, a magnetic exchange interaction generates singlet and triplet states. The $\chi_m T$ value shows a gradual increase as the temperature decreases, reaching a plateau (0.94 emu mol^{-1}) which is slightly below what would be anticipated for the triplet, and then decreases suddenly below 20 K. This observed temperature dependence of the $\chi_m T$ above 20 K is quite characteristic of a ferromagnetically coupled biradical. The magnetic data permit determination of the triplet−singlet energy gap arising from the intramolecular interaction. The least-squares fitting for the data by using a triplet−singlet model[24] ($H = -JS_1 \cdot S_2$) gives the best fit parameters J being 55.1(6) cm^{-1}, where the g value was fixed to be 2.0 and the intermolecular antiferromagnetic interaction ($\theta = -0.6(1)$ K) was included in the calculation. X- and Q band EPR spectra of a dilute frozen ethanol solution for **1** were measured at 5 K and did not show any significant feature,[25,26] where poorly resolved features around 1300 and 5400 G observed in the X band EPR spectrum might be due to the triplet signal.

[Ag^{I}(impy)$_2$](PF$_6$) (2). Figure 4 shows a plot of $\chi_m T$ versus T for **2**. The high-temperature $\chi_m T$ value (0.73 emu K mol^{-1}) is lower than that expected for two uncorrelated spins (0.75 emu K mol^{-1}). The $\chi_m T$ value steadily decreased as the temperature was lowered, reaching a minimum value of 0.64 emu K mol^{-1} at 19 K. X-ray analysis of **2** showed that an oxygen atom of the nitroxide group has a close contact (3.57(2) Å) with a nitrogen atom of the nitroxide in the adjacent molecule, which results in the antiferromagnetic behavior above 19 K. Below 19 K, a very abrupt rise in $\chi_m T$ is observed and the $\chi_m T$ value reached 0.716 emu K mol^{-1} at 2.5 K. The

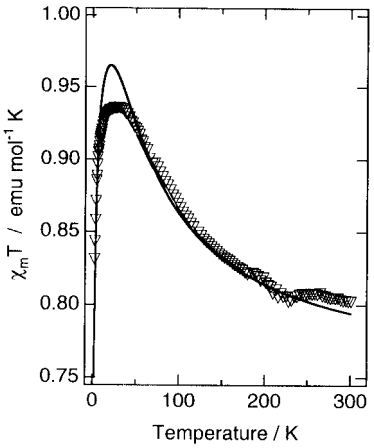

Figure 3. $\chi_m T$ versus T plots for [Cu^{I}(immepy)$_2$](PF$_6$) (×). The solid line corresponds to the best fit curves by using the parameters given in the text.

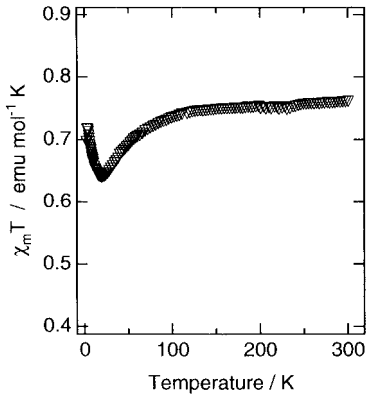

Figure 4. $\chi_m T$ versus T plot for [Ag^{I}(impy)$_2$](PF$_6$).

interpretation of the magnetic data requires the consideration of the intramolecular coupling of the two spins as well as the intermolecular coupling. The unusual abrupt rise in $\chi_m T$ below 19 K is due either to intramolecular ferromagnetic or to weakened antiferromagnetic interactions accompanied with a phase transition.

In order to gain further insight on the intramolecular magnetic interaction of **2**, the X-band EPR spectrum of a frozen ethanol solution at 5 K was measured (Figure 5). It exhibits an intense feature at 0.34 T with weak signals occurring at 0.29 and 0.38 T and a well-resolved half-field signal at 0.16 T. To interpret this spectrum quantitatively, the zero-field splitting parameters were calculated by using the reported method.[27] The $|D|$ and $|E|$ values obtained are 0.043 and 0.014 cm^{-1}, respectively. The relative intensity of the signal at 3370 G in the observed spectrum is larger than that for the simulated one; however, the origin of this is not understood yet. We have measured the temperature dependence of the signal intensity for $\Delta m = 2$ transition in the temperature range 10−80 K (Figure 6). The Curie plot gives a positive Weiss constant of $\theta = 4$ K. It should be noted that the intramolecular magnetic interaction is ferromagnetic. The gradual decrease of the $\chi_m T$ values in the high temperature region is due to the intermolecular antiferromagnetic interaction and the phase transition resulting in the inflection of $\chi_m T$ values at 19 K might lead to the weakened intermolecular antiferromagnetic interaction.

Electronic Spectra. The UV−visible absorption spectra of **1** and **2** along with the immepy ligand are depicted in Figure 7.

(24) Bleaney, B.; Bowers, K. D. *Proc. R. Soc. London, Ser. A* **1952**, *214*, 451.

(25) In the X-band EPR spectrum for **1**, a broad signal was observed in the region of $g = 1$. This signal was misassigned to a triplet signal with a large $|D|$ value;[26a] however, it turned out to be due to a unknown impurity.[26b]

(26) (a) Oshio, H.; Watanabe, T.; Ohto, A.; Ito, T., Ikoma, T.; Tero-Kubota, S. *Mol. Cryst. Liq. Cryst.* **1995**, *273*, 47. (b) Benelli, C.; Gatteschi, D. *Inorg. Chem.* **1982**, *21*, 1788.

(27) (a) Kottis, P.; Lefebvre, R. *J. Chem. Phys.* **1963**, *39*, 393. (b) Kottis, P.; Lefebvre, R. *J. Chem. Phys.* **1964**, *41*, 379.

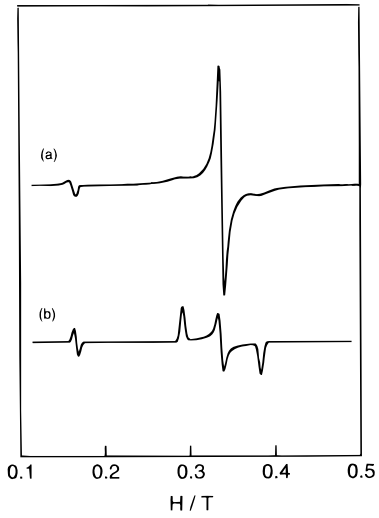

Figure 5. X-band EPR spectra of $[Ag^{I}(impy)_2](PF_6)$: (a) experimental spectrum in frozen ethanol solution at 5 K; (b) theoretical spectrum for a randomly oriented triplet system for given values of $|D|$ and $|E|$ in the text.

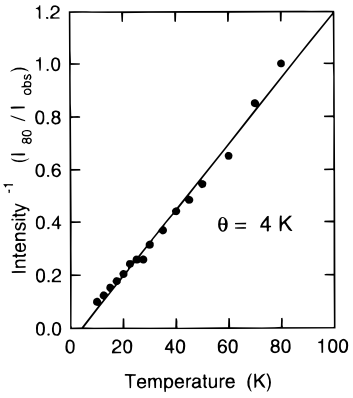

Figure 6. Reciprocal plots of EPR signal intensity due to $\Delta m = 2$ transition for $[Ag^{I}(impy)_2](PF_6)$ in frozen ethanol solution.

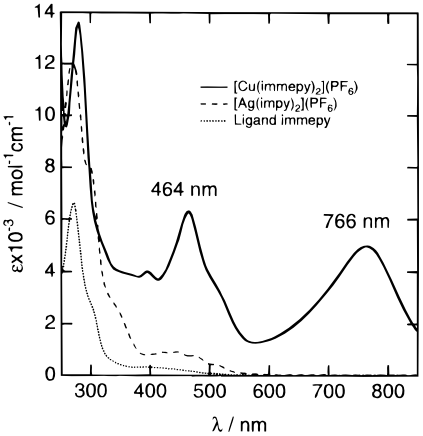

Figure 7. UV−vis spectra of (•••) immepy ligand, (—) $[Cu^{I}(immepy)_2](PF_6)$, and (---) $[Ag^{I}(impy)_2](PF_6)$ in acetonitrile.

In acetonitrile solution, $[Cu(immepy)_2]^+$ shows intense absorption bands at 766 nm (ϵ = 5000 M^{-1} cm^{-1}) and 464 nm (ϵ = 6300 M^{-1} cm^{-1}) with a shoulder band at 510 nm. These absorption bands were not observed in the spectra of immepy or $[Ag(impy)_2]^+$. The electronic spectra of Cu(I)−diimine systems have been well characterized by Müller et al.[28] $[Cu^{I}(TET)]^+$ (TET = 2,2′-bis(6-(2,2′-bipyridyl)biphenyl) exhibited an absorption band at 465 nm with a shoulder at 533 nm. If the coordination geometry about Cu ion is assumed to be pseudoterahedral (D_{2d}), the t_2 orbital of the Cu ion in T_d symmetry splits into $e(d_{xz},d_{yz})$ and $b_2(d_{xy})$ orbitals. Under D_{2d} symmetry, a combination of ligand π^* orbitals has e, a_2, and b_1 representations and the e orbital has the same symmetry as the e orbital of the Cu(I) ion. Therefore, for $[Cu(TET)]^+$, the intense band at 465 nm and shoulder at 533 nm were assigned to the $e(d_{xz},d_{yz}) \rightarrow e(\pi^*)$ and $b_2(d_{xy}) \rightarrow e(\pi^*)$ transitions, respectively.[28] On the other hand, a Cu(I) complex with an *o*-semiquinone ligand, $[Cu^{I}_2\{\mu\text{-}N_2[CO(OBu^t)]_2[\mu\text{-}Ph_2P(CH_2)_6PPh_2\}_2]BPh_4$[29] shows an intense absorption band at 700 nm and this band was assigned to a metal to ligand charge-transfer band ($d_{xy} \rightarrow \pi_1^*$).[30]

Scheme 1

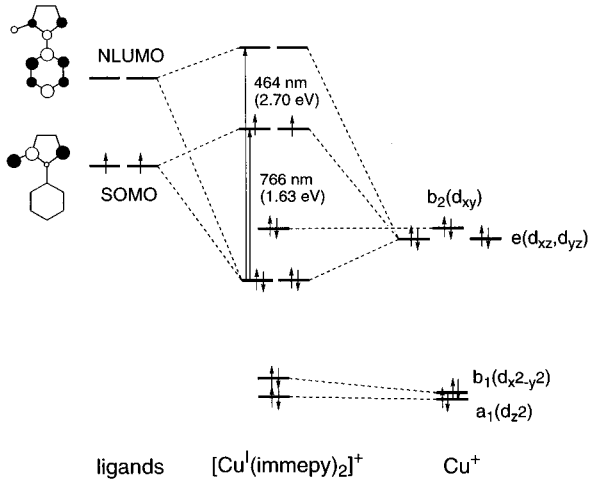

A PM3 molecular orbital calculation for the ligand immepy (where the imino nitroxide fragment and the pyridine ring are coplanar) has been done in order to clarify the electronic structure of immepy. This calculation shows that the singly occupied molecular orbital (SOMO) is centered mainly on the imino nitroxide fragment, while the next lowest unoccupied orbital (NLUMO) is delocalized on the whole π system. Both the SOMO and the NLUMO are of proper symmetry to overlap with the d_{xz} and d_{yz} orbitals. If, by analogy to $[Cu(TET)]^+$, we assume pseudotetrahedral geometry (D_{2d}) for **1**, the lower energy band (766 nm) would correspond to a $e(d_{xz},d_{yz}) \rightarrow$ SOMO transition, the higher energy band (464 nm; 2.70 eV) to $e(d_{xz},d_{yz}) \rightarrow$ NLUMO, and the shoulder at 510 nm (2.43 eV) to $b_2(d_{xy}) \rightarrow$ NLUMO. Hence, the $e(d_{xz},d_{yz})$ and $b_2(d_{xy})$ orbitals apparently split with an approximate energy separation of 0.27 eV (=2.70 − 2.43 eV) (Scheme 1). It should be noted that the lack of such metal to ligand charge-transfer bands in the silver complex **2** is supposed to be due to the large energy separation between the metal d and ligand π^* orbitals.

Electrochemistry. The electrochemical properties of **1**, **2**, and immepy were studied by cyclic voltammetry. Cyclic voltammograms (CV), between −1.25 to +1.25 V, are illustrated in Figure 8, and the redox potentials (vs Ag/AgCl) are summarized in Table 4.

In the cyclic voltammogram of immepy (Figure 8a), a reversible wave corresponding to the immepy/immepy$^-$ couple appears at $E_{1/2}$ = −0.73 V (ΔE_p = 75 mV). In addition, an irreversible oxidation wave appears at 1.23 V. The cyclic voltammogram of $[Cu^{I}(immepy)_2]^+$ (Figure 8b) shows fairly reversible waves at −0.59 V (ΔE_p = 75 mV), −0.31 V (ΔE_p

(28) Müller, E.; Piguet, C.; Bernardinelli, G.; Williams, A. F. *Inorg. Chem.* **1988**, *27*, 849.

(29) Moscherosch, M.; Field, J. S.; Kaim, W.; Kohlmann, S.; Krejcik, M. *J. Chem. Soc., Dalton Trans.* **1993**, 211.

(30) Vogler, C.; Hausen, H.-D.; Kaim, W.; Kohlmann, S.; Kramer, H. E. A.; Rieker, J. *Angew. Chem.* **1989**, *101*, 1734.

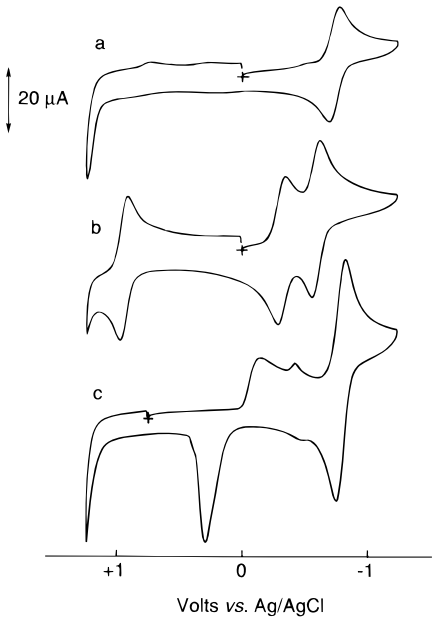

Figure 8. Cyclic voltammograms on a glassy carbon electrode in 0.1 M CH_3CN, solution of [N(t-Bu)$_4$]PF_6, at scan rate of 100 mV/s vs Ag/AgCl: (a) immepy ligand; (b) [Cu^I(immepy)](PF_6); (c) [Ag^I(impy)$_2$]-(PF_6).

Table 4. Electrochemical Data[a]

compd	$E_{1/2}$, V (ΔE_p, mV)
immepy	−0.73 (80)
	1.23[b]
	1.53[b]
[Cu(immepy)$_2$](PF_6)	−0.59 (70)
	−0.31 (60)
	0.95 (80)
	1.37[b]
	1.61[b]
[Ag(impy)$_2$](PF_6)	−0.78 (70)
	−0.13[b]
	−0.41[b]
	0.32[b]

[a] Glassy carbon electrode, Pt auxiliary electrode, Ag/AgCl reference electrode. All solutions purged with N_2 prior to use. Electrolyte: 0.1 M tetra-*tert*-butylammonium hexafluorophosphate. $E_{1/2} = (E_c + E_a)/2$; $\Delta E_p = E_c - E_a$ (in mV); E_c and E_a = peak potentials for reduction and oxidation. [b] Irreversible wave.

= 60 mV), and 0.95 V (ΔE_p = 75 mV). Two reversible waves at −0.59 and −0.31 V can be assigned as being due to one-electron reductions of each coordinated ligand, where a peak separation of 280 mV yields a comproportionation constant $K_c = 5.5 \times 10^4$. The two step reductions of the ligands in **1** result from electronic and electrostatic interactions between the coordinated ligands. The wave at 0.95 V is assumed to be a metal-based Cu^I/Cu^{II} oxidation wave, where such a wave was not observed in the cyclic voltammogram of the free immepy ligand. A comparison of the relative peak areas for the ligand reductions and the one-electron Cu(II)/Cu(I) couple is consistent with this assumption. The electrochemical process for **1** can be summarized by the following equations:

$$[Cu^{II}(immepy)_2]^{2+} \overset{-1e^-}{\rightleftharpoons} [Cu^{I}(immepy)_2]^{+} \overset{+2e^-}{\rightleftharpoons} [Cu^{I}(immepy^-)_2]^-$$

Electrochemical redox processes in **1** are related to reduction and oxidation involving the SOMO and $b_2(d_{xy})$, respectively. The difference (1.26 V) between the oxidation potential (0.95 V) of the Cu^+ ion and the first reduction potential (−0.31 V) of the ligand in **1** may be compared with the orbital energy difference between the SOMO and the $b_2(d_{xy})$ as measured by the metal-to-ligand charge-transfer absorption energy of **1**.[31] In acetonitrile solution, the charge-transfer band for the $e(d_{xz},d_{yz})$ → SOMO transition was observed at 766 nm (1.63 eV), while the energy separation between the $b_2(d_{xy})$ and $e(d_{xz},d_{yz})$ is about 0.27 eV as estimated from the charge-transfer bands; i.e., $e(d_{xz},d_{yz})$ → NLUMO (460 nm: 2.70 eV) and $b_2(d_{xy})$ → NLUMO (510 nm: 2.43 eV). This would require the splitting between the $b_2(d_{xy})$ and SOMO to be 1.36 V. This small discrepancy of 0.1 V is indicative of a system showing inner-sphere rearrangements following the electrochemical process like distortion to the square planar geometry accompanied by the oxidation of Cu ion.

In Figure 8c is illustrated a cyclic voltammogram of [Ag-(impy)$_2$]$^+$. In the reductive scan, a broad Ag^+ reduction wave appears at −0.13 V. It is followed by the impy-based reduction at −0.78 V (ΔE_p = 70 mV). The reoxidation wave of the Ag^0/Ag^+ couple occurred at $E_{p,a}$ = 0.32 V in the reversed scan. It should be noted that repetitive scans between +0.75 and 0 V show no Ag^0/Ag^+ coupled wave. For **2**, the reductive scan to −1.25 V results in reduction to Ag^0 accompanied by dissociation of impy which is subsequently reduced.

$$[Ag^{I}(impy)_2]^+ \xrightarrow{+e^-} Ag^0 + 2impy \xrightarrow{+2e^-} Ag^0 + 2impy^-$$

It should be noted that the oxidation wave corresponding to the Ag^+/Ag^{2+} couple was not observed in the oxidative scan to 1.25 V.

Discussion

The results reported here show that (pseudo)tetrahedral coordination of the two imino nitroxides to Cu(I) and silver(I) ions leads to ferromagnetic interactions. [Cu^I(immepy)$_2$](PF_6) (**1**) complex showed especially strong ferromagnetic interaction which can be attributed to the charge-transfer interaction. Complex **1** showed a strong absorption band at 766 nm which corresponds to electron transfer from the $e(d_{xz},d_{yz})$ orbital to the SOMO (radical). The π-back-donation, which mixes the $e(d_{xz},d_{yz})$ orbital and SOMO, induces a large spin delocalization of each ligand radical onto the Cu(I) ion; the resultant spin on the Cu ion creating in the strong ferromagnetic interaction.

The mechanism which determines the relative energies (J) of the triplet and singlet states has been often discussed in terms of the Heitler-London interaction and valence bond configuration interaction between the ground and charge-transfer states.[32] J depends primarily on the Heitler−London type interaction within the ground state, and in natural magnetic orbital treatments the triplet−singlet energy gap is expressed as

$$J_{GS} = 2K_{\pi^*\pi^*} + 4\beta_{\pi^*\pi^*}S_{\pi^*\pi^*}$$

where $K_{\pi^*\pi^*}$, $\beta_{\pi^*\pi^*}$, and $S_{\pi^*\pi^*}$ represent the two electron exchange, transfer, and overlap integrals between radical SOMOs, respectively. In **1**, the two coordinated radicals are orthogonally arranged. As a result, $S_{\pi^*\pi^*}$ is zero and the strong ferromagnetic coupling in **1** primarily arises from the two-electron exchange integral, $2K_{\pi^*\pi^*}$. Compound **1**, however, showed a fairly strong charge-transfer band which corresponds

(31) (a) Dodsworth, E. S.; Lever, A. B. P. *Chem. Phys. Lett.* **1985**, *119*, 61. (b) Dodsworth, E. S.; Lever, A. B. P. *Chem. Phys. Lett.* **1986**, *124*, 152.
(32) (a) Kahn, O. *Molecular Magnetism*; VCH Publishers: Weinheim, New York, 1993. (b) Seggern, I.; Tuczek, F.; Bensch, W. *Inorg. Chem.* **1995**, *34*, 5530. (c) Tuczek, F.; Solomon, E. I. *J. Am. Chem. Soc.* **1994**, *116*, 6916.

to the π-back-donation to the radical SOMO. It is necessary to consider a valence bond configuration interaction to interpret the ferromagnetic interaction.

Valence bond-like treatments have been invoked to explain ferromagnetic interactions or ordering in metal complexes as well as in pure organic compounds. For example, Goodenough proposed that interactions between half-filled orbitals on one metal and empty orbitals on the other metal can contribute to ferromagnetic interactions.[33] This mechanism was also invoked to justify the ferromagnetic ordering observed for (*p*-nitrophenyl)nitronyl nitroxide[34] and ferromagnetic interactions in $[Mn^{III}(\mu\text{-}O)(\mu\text{-}CH_3CO_2)_2Mn^{III}]$[35] and $[Gd_2Cu_4]$[36] complexes. The situation in **1** is not the same as the above case but is closer to the models by McConnel and Breslow.[37] We assume pseudo-tetrahedral coordination geometry (D_{2d}) about Cu ion for **1** and use the orthogonal orbitals in the following treatment. Within the four-orbital (degenerate e(d_{xz},d_{yz}) and degenerate π^* orbitals) and six-electron (four on e(d_{xz},d_{yz}) and two on each π^*) system, the ground triplet (GS_T) and singlet (GS_S) configurations for **1** are represented by

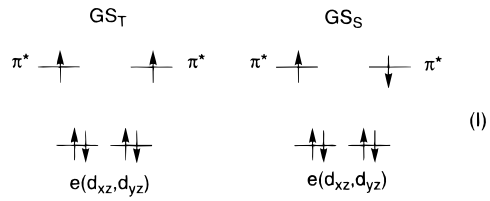

where GS_S has a complement spin configuration. The MLCT configuration generated by the CT transition from e to π^* is represented by

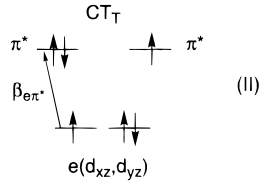

where $\beta_{e\pi^*}$ is a transfer integral. This MLCT state has both triplet (CT_T) and singlet (CT_S) configurations. However, the triplet is lower in energy than the singlet due to the orthogonality of the singly occupied e and π^* orbitals. The mutual repulsion between the ground and MLCT states leads to a mixing between the two configurations. The admixed triplet and singlet ground states are stabilized by $-2\beta_{e\pi^*}{}^2/(\Delta - K_{e\pi^*})$ and $-2\beta_{e\pi^*}{}^2/(\Delta + K_{e\pi^*})$, respectively, where Δ is the cost in energy of transferring an electron from e to π^* and $K_{e\pi^*}$ is the interatomic exchange integral involving the orbitals e and π^*. As a consequence of mixing, the triplet is lower than the singlet and the triplet−singlet energy gap J is

$$J = \frac{4\beta_{e\pi^*}{}^2 K_{e\pi^*}}{\Delta^2 - K_{e\pi^*}{}^2}$$

There is the more excited charge-transfer configuration. Starting from the MLCT configuration (II), an electron on a doubly occupied e orbital can be transferred to a singly occupied π^* orbital with the result that the Cu ion possesses singly occupied orbitals. By comparison with the GS configuration (I), this corresponds to a double charge-transfer configuration, and this configuration should be a triplet due to the Hund's rule.

Scheme 2

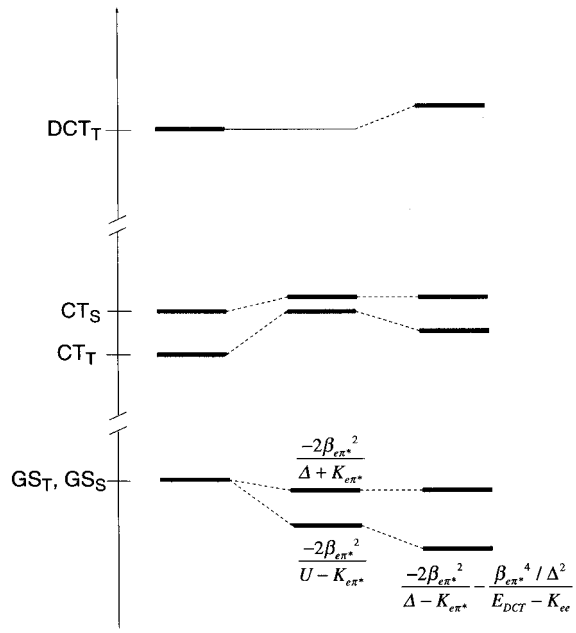

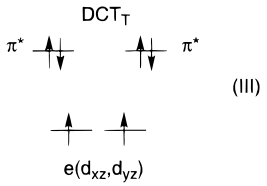

The interaction between the GS and DCT configurations stabilizes the GS triplet, because the singlet DCT configuration is quite high in energy. The resulting stabilization of the GS_T is $-(\beta_{e\pi^*}{}^4/\Delta^2)/(E_{DCT} - K_{ee})$, where E_{DCT} and K_{ee} represent the energy cost associated with this electron transfer and the one-site exchange integral, respectively. Stabilization due to the double charge transfer is, in general, very small. In this case, however, the two unpaired electrons locate on the Cu ion in the DCT configuration, which leads to the fairly large exchange integral K_{ee}. Hence, it can be expected that the GS_T−DCT_T configuration interaction cannot be ignored. As the result of the configuration interaction of the GS_T with CT_T and DCT_T, the GS_T is stabilized by $-2\beta_{e\pi^*}{}^2/(U - K_{e\pi^*}) - (\beta_{e\pi^*}{}^4/\Delta^2)/(E_{DCT} - K_{ee})$.[38] Scheme 2 summarizes these configuration interactions.

The magnetic interaction in $[Ag^I(impy)](PF6)$ (**2**) is quite different from that in **1**. In **2**, the coordination geometry about silver ion deviates from a tetrahedron and this leads to the broken orthogonality of the coordinating imino nitroxides. Furthermore, compound **2** did not show any metal to ligand charge-transfer bands in the UV−visible region and the oxidation wave

(33) Goodenough, J. B. *Magnetism and the Chemical Bond*; Interscience: New York, 1963.
(34) Tamura, M.; Nakazawa, Y.; Shiomi, D.; Nozawa, K.; Hosokoshi, Y.; Ishioka, M.; Takahashi, M. Kinoshita, M. *Chem. Phys. Lett.* **1991**, *86*, 401.
(35) Hotzelmann, R.; Wieghardt, K.; Flörke, U.; Haupt, H.-J.; Weatherburn, D. C.; Bonvoisin, J.; Blondin, G.; Gierard, J.-J. *J. Am. Chem. Soc.* **1992**, *114*, 1681.
(36) Andruh, M.; Ramade, I.; Codjovi, E.; Guillou, O.; Kahn, O.; Trombe, J. C. *J. Am. Chem. Soc.* **1993**, *115*, 1822.
(37) (a) McConnel, H. M. *Proc. Robert A. Welch Found. Conf. Chem. Res.* **1976**, *11*, 144. (b) Breslow, R.; Juan, B.; Kluttz, R. Q.; Xia, C. Z. *Tetrahedron* **1982**, *38*, 863. (c) Breslow, R. *Pure Appl. Chem.* **1982**, *54*, 927.
(38) (a) Tuczek, F.; Solomon, E. I. *Inorg. Chem.* **1993**, *32*, 2850. (b) Shen, Z.; Allen, J. W.; Yeh, J. J.; Kang, J.-S.; Ellis, W.; Spicer, W.; Lindau, I.; Maple, M. B.; Dalichaouch, Y. D.; Torikachvili, M. S.; Sun. J. Z.; Geballe, T. H. *Phys. Rev. B* **1987**, *36*, 8414.

corresponding to the Ag(I)/Ag(II) couple was not observed. Compound **1** showed the oxidation wave for the Cu(I)/Cu(II) couple at 0.95 V (vs Ag/AgCl). Therefore, there is an apparent energy mismatch between the ligand π^* and the silver ion d orbital. It can be concluded that not only the broken orthogonality, but also the lack of configuration interactions stabilizing the high-spin state, make the ferromagnetic interaction weak in the case of **2**.

Conclusion

In the design of magnetic materials, metal ions have been often regarded and used as a source of spins. Recently, we have reported that a diamagnetic Pd(II) ion propagates a strong antiferromagnetic interaction ($J = -168$ cm^{-1}; $H = -JS_1 \cdot S_2$) in *trans*-[$PdCl_2$(immepy)$_2$], which showed a MLCT band (d_{xy} to SOMO) at 500 nm ($\epsilon = 1800$ M^{-1} cm^{-1}).[39] Under the square planar coordination geometry of the Pd(II) ion, indirect overlap of the radical SOMOs through the d_{xy} orbitals leads to the antiferromagnetic interaction. In this paper we showed that coordination geometry characteristic of d^{10} metal ions provides an orthogonal arrangement of two imino nitroxides and this leads to ferromagnetic interaction. It should be noted that the charge-transfer interaction not only in the Cu(I) but also Pd(II) systems plays an important role in the propagation of magnetic interaction. The strong ferromagnetic interaction observed in the Cu(I) imino nitroxides indicates that the Cu(I) ion is undoubtedly useful for the joints of radical networks, where each radical component can be ferromagnetically connected. We are currently attempting to design multidentate radical ligands which are able to bridge two Cu(I) ions.

Acknowledgment. The authors thank Prof. D. Gatteschi (Università di Firenze) for his valuable comments on EPR spectra. This work was in part supported by The Morino Fundation.

Supporting Information Available: Table of crystal data (Tables S1 and S5), positional parameters (Tables S2 and S6), anisotropic thermal parameters (S3 and S7), and complete bond length and angles (Tables S4, S8, and S9), as well as packing diagrams data (15 pages). Ordering information is given on any masthead page.

IC960939E

(39) Oshio, H.; Ohto, A.; Ito, T. *J. Chem. Soc., Chem. Commun*. **1996**, 1541.